Physica E 41 (2009) 1757–1762

Contents lists available at ScienceDirect

Physica E

journal homepage: www.elsevier.com/locate/physe

Effect of the synthesis route on the structural properties and shape of the indium oxide (In_2O_3) nano-particles

M.-M. Bagheri-Mohagheghi [a], N. Shahtahmasebi [b], E. Mozafari [b], M. Shokooh-Saremi [c,*]

[a] Department of Physics, Damghan University of Basic Sciences, Damghan, Iran
[b] Nanotechnology Research Center, Department of Physics, School of Basic Sciences, Ferdowsi University of Mashhad, Iran
[c] Department of Electrical Engineering, University of Texas at Arlington, USA

ARTICLE INFO

Article history:
Received 20 October 2008
Received in revised form
19 May 2009
Accepted 14 June 2009
Available online 21 June 2009

PACS:
78.67.Bf
61.46.Df
61.05.Cp

Keywords:
Nano-particles
Indium oxide
Sol–gel technique
Hydro-thermal technique
Characterization

ABSTRACT

Nano-crystalline indium oxide (In_2O_3) particles have been synthesized by sol–gel and hydro-thermal techniques. A simple hydro-alcoholic solution consisting indium nitrate hydrate and citric acid (in sol–gel method) and 1, 4-butandiol (in hydro-thermal method) have been utilized. The structural properties of indium oxide nano-powders annealed at 450 °C (for both methods) have been characterized by the X-ray diffraction (XRD), transmission electron microscopy (TEM), scanning electron microscopy (SEM), and specific surface area (SSA) analysis. Structural analysis of the samples shows cubic phase in sol–gel and cubic-hexagonal phase mixture in hydro-thermally prepared particles. The nano-particles prepared by sol–gel method have nearly spherical shape, whereas hydro-thermally-made ones display wire- and needle-like shape in addition to the spherical shape. The obtained In_2O_3 nano-particles surface areas were 23.2 and 55.3 in sol–gel and hydro-thermal methods, respectively. The optical direct band gap of In_2O_3 nano-particles were determined to be ~4.32 and ~4.24 eV for sol–gel and hydro-thermal methods, respectively. These values exhibit ~0.5 eV blue shift from that the bulk In_2O_3 (3.75 eV), which is related to the particle size reduction and approaching the quantum confinement limit of nano-particles.

1. Introduction

Indium oxide (In_2O_3) is a wide band gap n-type semiconductor with direct and indirect band gaps of 3.75 and 2.6 eV, respectively. In_2O_3 is an insulator in stoichiometric state, but behaves as a high conductive semiconductor in its non-stoichiometric state. Single crystal In_2O_3 has cubic bixebyte structure (also called as c-type rare-earth oxide structure) with lattice parameter of 10.117 Å [1,2]. Furthermore, indium oxide is an important and well-known transparent conducting oxide (TCO). Over the past decades, many studies have been done on preparation of indium oxide (IO) and indium tin oxide (ITO) in bulk or thin film form, which are of the most important technical materials for various applications such as solar cells, sensor modules, and transparent electrode materials for opto-electronic devices [2–4].

The recent studies on the un-doped and doped indium oxide have been mainly concentrated on preparation of various nano-structural shapes and their properties. For practical applications, a significant interest has been shown on the field of zero-dimensional and one-dimensional semiconducting indium oxide and indium tin oxide, such as nano-spheres [5], nano-rods [6], nano-wires [7], and nano-tubes [8].

There is a variety of synthesis techniques (routes) for preparation of indium oxide nano-particles such as sol–gel [6], hydro-thermal [7,9], co-precipitation [5,6,10], and emulsion [11]. Amongst these methods, the sol–gel and hydro-thermal processes have been widely used due to their simplicity, lower cost, and ability to control the particle size and shape.

Since fabrication parameters highly affect the structural properties of the nano-particles [12,13], depending on the synthesis route and conditions, a variety of morphologies, different shapes, and phase structures are obtainable [14,15].

In this paper, we report preparation and study of the structural properties of indium oxide nano-particles by two synthesis methods i.e., sol–gel and hydro-thermal. The structural and shape characterization of nano-particles (powders) has been performed by the X-ray diffraction (XRD), scanning and transmission electron microscopy (SEM and TEM), electron diffraction, and specific surface area (SSA) analysis. The optical band gap of the prepared nano-particles has been determined by the UV–vis optical absorption measurements for both synthesis techniques.

* Corresponding author.
E-mail addresses: saremi@uta.edu, mssaremi@yahoo.com (M. Shokooh-Saremi).

1386-9477/$ - see front matter © 2009 Elsevier B.V. All rights reserved.
doi:10.1016/j.physe.2009.06.009

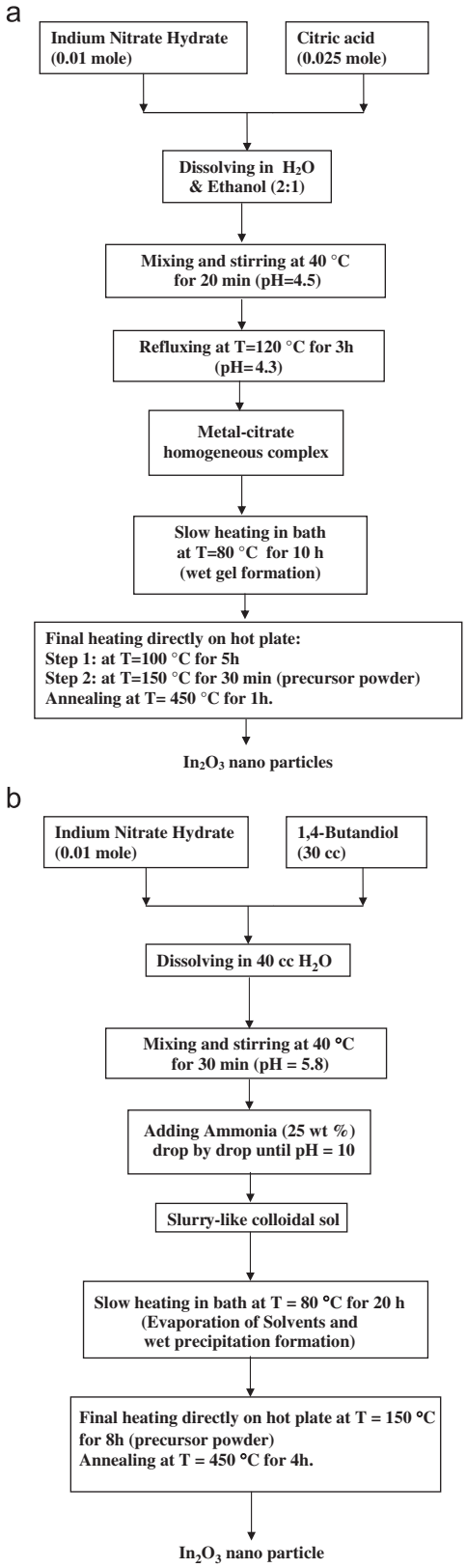

Fig. 1. The flow charts for preparation of In_2O_3 nano-particles by (a) sol–gel and (b) hydro-thermal processes.

2. Experimental details

2.1. Synthesis of In_2O_3 nano-particles by sol–gel and hydro-thermal methods

In_2O_3 nano-particles were synthesized by two methods: (A) complex sol–gel, and (B) Hydro-thermal; as summarized by flow charts in Figs. 1(a) and (b), respectively. First, a sol solution consisting indium (III) nitrate hydrate (as inorganic basic reactant), double-distilled water and ethanol (as solvent), with specific weight percentages, was prepared.

As shown in Fig. 1(a), citric acid (as complexing agent) was added to the initial solution and the resulting mixture was stirred and dissolved at 40 °C for 20 min until a clear solution was

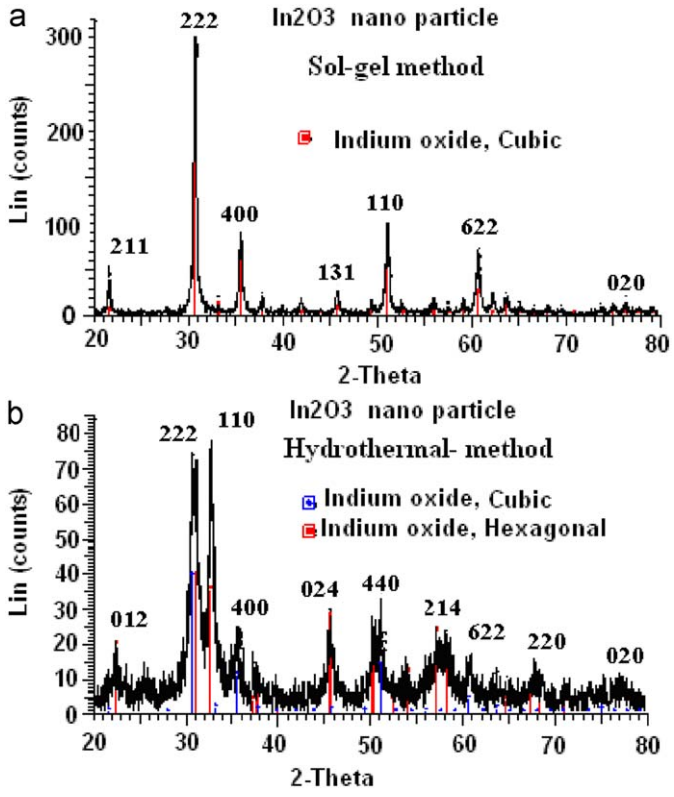

Fig. 2. The XRD patterns of the In_2O_3 nano-particles annealed at $T = 450$ °C for (a) sol–gel and (b) hydro-thermal processes.

Table 1
The XRD parameters and particle mean size in different crystallographic orientations for nano-particles prepared by sol–gel and hydro-thermal methods.

hkl	2θ (degree)	*d* (Å)	Intensity (Cps)	FWHM (degree)	Particle mean size (nm)	Identification with (*h k l*) value
Sol–gel method						
222	30.626	2.91682	303	0.360	25.3	In_2O_3-cubic
400	35.501	2.52661	89.2	0.396	23.4	In_2O_3-cubic
440	51.08	1.78667	102	0.411	23.8	In_2O_3-cubic
622	60.615	1.52644	68.2	0.420	24.3	In_2O_3-cubic
Hydro-thermal method						
222	30.63	2.91645	79.4	0.797	11.4	In_2O_3-cubic
110	32.654	2.74014	73.2	0.523	17.5	In_2O_3-hexagonal
400	35.518	2.52546	25	0.200	46.3	In_2O_3-cubic
024	45.7	1.98366	28.1	0.316	30.3	In_2O_3-hexagonal
116	50.176	1.8167	28	0.328	29.7	In_2O_3-hexagonal
440	51.115	1.7855	32.6	0.147	66.5	In_2O_3-cubic

obtained (pH = 4.5). This solution was refluxed at $T = 120\,^{\circ}C$ for 3 h (pH = 4.3). During refluxing, the solution turned into a metal-citrate homogeneous complex with a slight color change from clear to light green. After cooling down, for both completion of the reactions required for development of the complex and evaporation of the solvent, the sol was further slowly heated at $T = 80 \pm 5\,^{\circ}C$ for 10 h in an open bath until a green wet gel was obtained. During continued heating at this temperature, the chelating between metal cations (In^{3+}) and citric acid as complexing agent is developed [16]. This step helps achieving a proper stoichiometry and control of the particle size without any need to a special atmosphere. In addition, this improves uniformity of the distribution of the metal cations in the solution. In the final step of the sol–gel process, the wet gel was fully dried by direct heating on the hot plate at $T = 100\,^{\circ}C$ and $150\,^{\circ}C$ for 5 h and 30 min, respectively. The resulting product was a light-yellow porous gel as xerogel.

In method (B), as shown in Fig. 1(b), 0.01 mole indium nitrate hydrate (3 g) was dissolved in 40 cc double-distilled water and 30 cc 1,4-butandiol as dispersing agent [9,17]. Then, the solution was stirred for 30 min at $T = 40\,^{\circ}C$ with pH = 5.8. Ammonia (25 wt%) was added drop by drop to the solution to achieve a final pH = 10 at room temperature. After formation of a white slurry-like colloidal sol, it was further slowly heated at $T = 80 \pm 5\,^{\circ}C$ for 10 h in an open bath until a light-brown wet solid precipitation was obtained by evaporation of the solvents. In this hydro-thermal process, essential chemical reactions take place between In^{3+} ions and ammonia (as mineralizer), for preparation of the

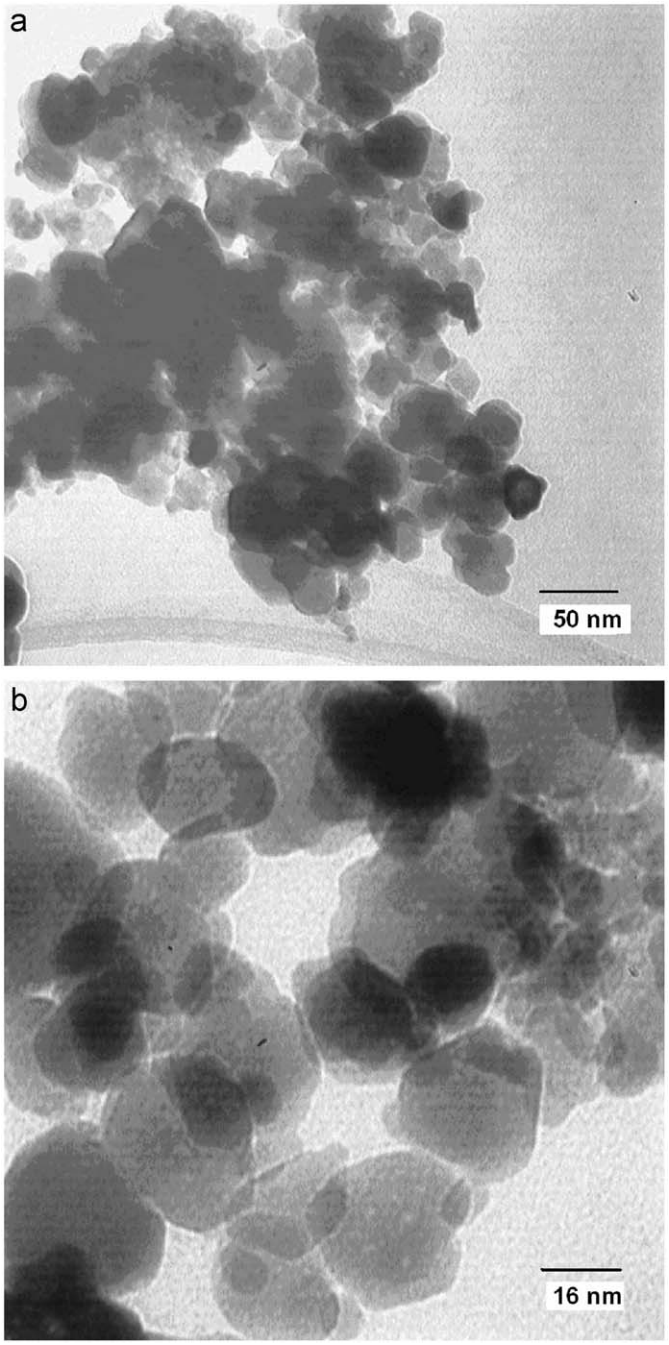

Fig. 3. The TEM images of In_2O_3 nano-particles prepared by the sol–gel method (with two different magnifications).

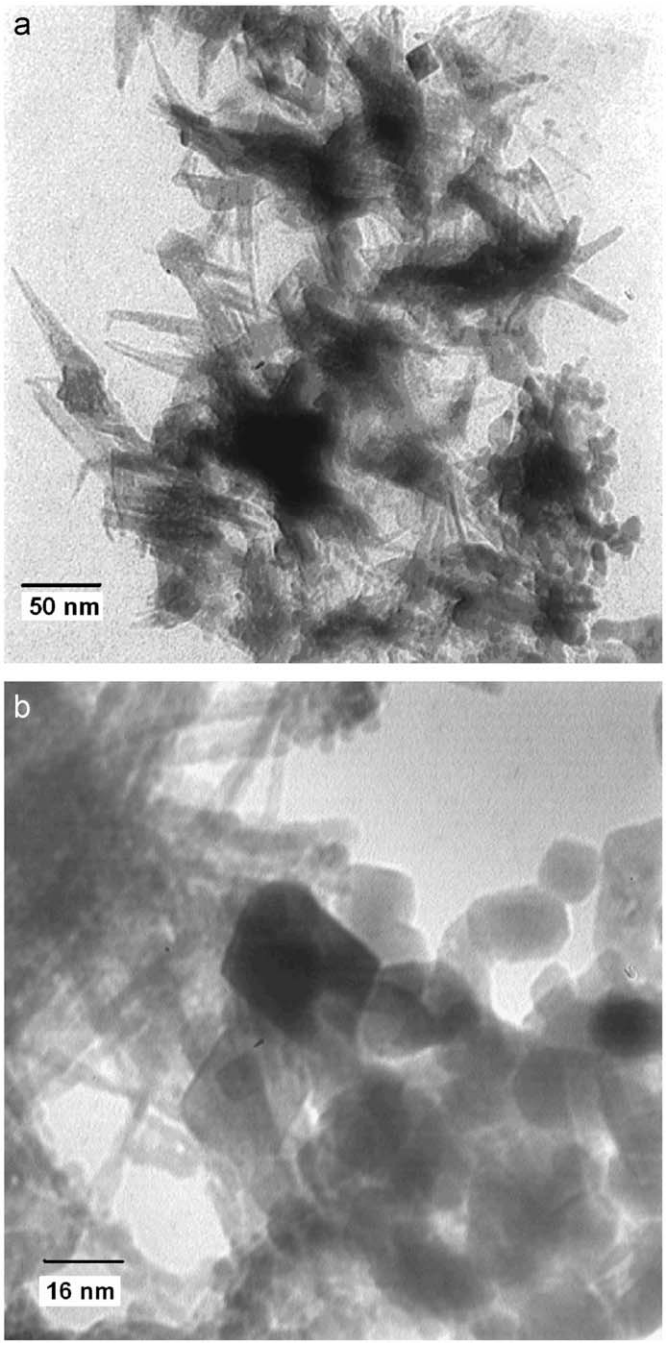

Fig. 4. The TEM images of In_2O_3 nano-particles prepared by the hydro-thermal method (with two different magnifications).

In_2O_3 powders [18]. In the final stage, the wet precipitation was fully dried by direct heating on the hot plate at $T = 150\,^{\circ}C$ for 8 h. A white–grey powder was the final product.

2.2. Post-annealing of the In_2O_3 nano-powders

The precursor powders obtained by both techniques were grounded in the glassy mortar to be turned into fine powders. Then, powders were heated in a Pyrex crucible to $T = 450\,^{\circ}C$ and calcined for 1 h (for method A) and 4 h (for method B), respectively, in an electric box furnace, and finally cooled down to room temperature. By post-annealing of the powders (in both methods), all of the organic compounds were completely decomposed and In_2O_3 nano-particles obtained.

2.3. Characterization of nano-particles (powders)

The X-ray diffraction patterns of In_2O_3 nano-powders, prepared by the hydro-thermal and sol–gel processes, were recorded by D8 Advance Bruker system using Cu K_α ($\lambda = 0.154056$ nm) radiation with 2θ ranging 20–70°. Transmission electron microscopy micrographs and electron diffraction patterns of the prepared In_2O_3 nano-powders were obtained using a LEO 912 AB system operating at 120 kV. The morphology of the nano-powders was analyzed by scanning electron microscopy using a LEO 1450 VP system. The samples for TEM analysis were prepared by dispersing the In_2O_3 nano-powders in acetone using an ultrasound bath. A drop of this dispersed suspension was put onto 200-mesh carbon-coated Cu grids and then dried in vacuum.

The BET surface area of nano-powders was evaluated by N_2 adsorption isotherm measurements at 77 K by a Quantachrome Autoadsorb1 system. Before each measurement, samples were degassed at 150 °C under vacuum (10^{-3} mmHg) for 16 h. Also, the optical absorption measurements of powders in range of 190–1100 nm were recorded using a UV–vis single beam spectrophotometer (Agilent 8453) for determining the optical band gap.

3. Results and discussion

The XRD patterns of In_2O_3 nano-powders prepared by sol–gel (A) and hydro-thermal (B) methods have been shown in Figs. 2(a) and (b). It is clear that the crystalline peaks in the XRD pattern in Fig. 2(a) for synthesis route (A) are in a good agreement with the diffraction data of cubic indium oxide ($a = 10.118$ Å) from JCPDS card. The intensity of diffraction peak corresponding to the (2 2 2) orientation is higher than the other peaks. The other peaks corresponding to (2 1 1), (4 0 0), (4 4 0), and (6 2 2) orientations are also observed with lower intensity. The XRD pattern in Fig. 2(b)

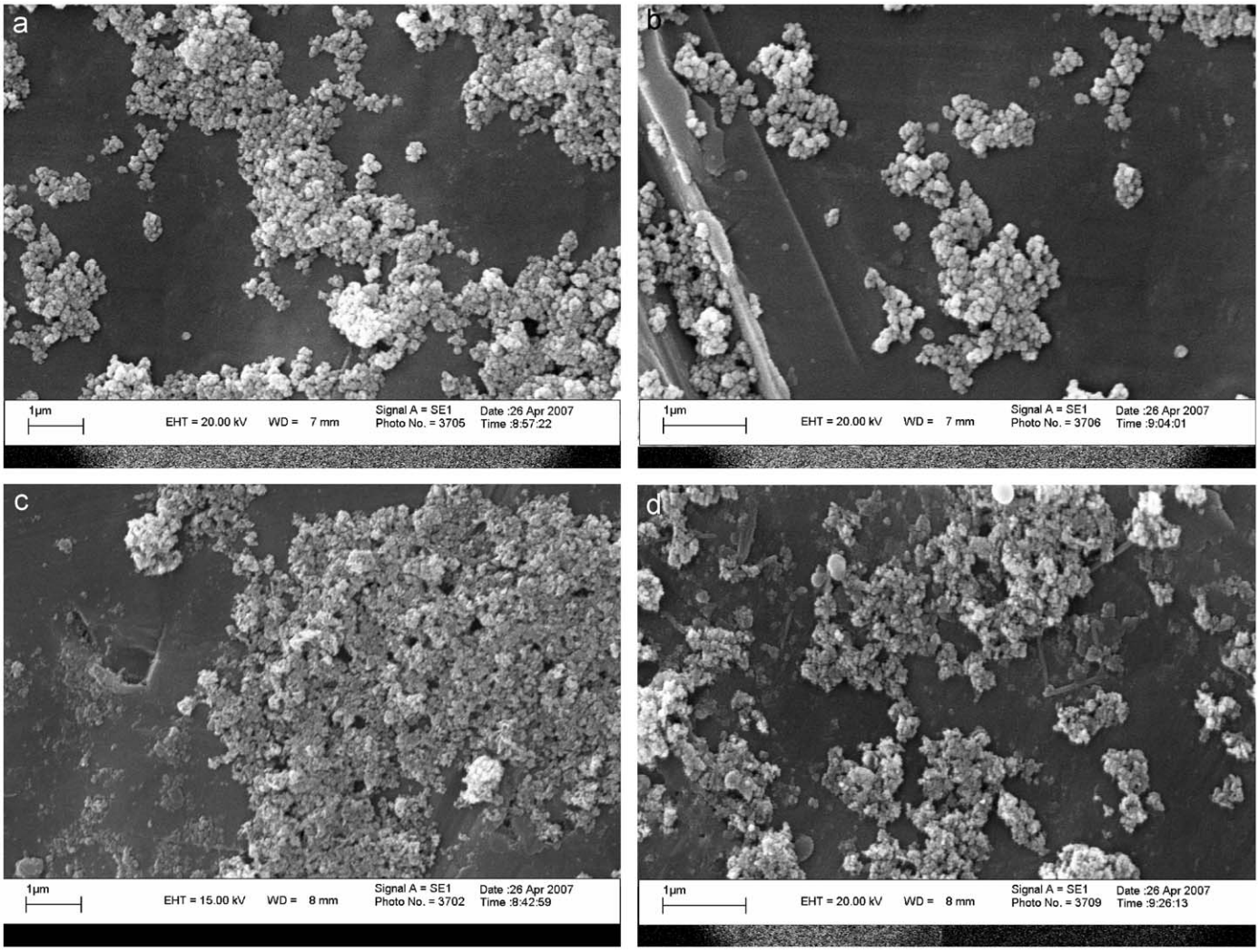

Fig. 5. The SEM images of In_2O_3 nano-particles prepared by (a) sol–gel (magnification 20 K), (b) sol–gel (magnification 30 K), (c) hydro-thermal (magnification 20 K), and (d) hydro-thermal (magnification 30 K) methods.

for synthesis route (B) shows a cubic-hexagonal mixed phase in In_2O_3 lattice structure that indicates a structural phase transition, mainly due to the smaller size of nano-particles and quantum confinement effect. Indeed, in the hydro-thermal method, XRD peaks of In_2O_3 nano-particles are broadened in comparison to the nano-particles prepared by the sol–gel method. In addition, structural characterization of nano-particles prepared by the two synthesis methods is given in Table 1. As seen, In_2O_3 nano-particles prepared by the sol–gel method with pure cubic phase have narrower peaks and higher intensity compared to those prepared by hydro-thermal method with hexagonal-cubic mixed phase. This indicates that the mean size of nano-crystallites in method (B) is smaller than those obtained by method (A).

The TEM micrographs of the In_2O_3 nano-powders prepared by sol–gel and hydro-thermal methods have been shown in Figs. 3 and 4, respectively. Figs. 3(a) and (b) exhibit nano-sized In_2O_3 particles with size range from 10 to 45 nm. The shape of the nano-particles is nearly spherical with an almost homogeneous distribution. The TEM images in Figs. 4(a) and (b) confirm the nano-metric size of the particles as branches in range of 3–20 nm in sectional diameter. As illustrated in Fig. 4(b), there are a large number of wire-like or needle-like structures in addition to the nano-crystallites with cubic-hexagonal sections. The nano-wires have a length about 15–25 nm, and a width of about 3–5 nm. Thus, the difference in morphology characteristics of the In_2O_3 particles prepared by sol–gel and hydro-thermal methods in Figs. 3 and 4 implies that the type of the synthesis route plays a crucial role in determining the morphology of particles [19,20].

The SEM images of the In_2O_3 nano-particles prepared by sol–gel and hydro-thermal methods have been shown in Fig. 5 (with different magnifications). As seen, nano-particles prepared by both methods have been grown as individual clusters, but order and distribution of nano-particles obtained by the method (A) is better than of the method (B). Indeed, in sol–gel method using the citric acid as complexing or polymerizing agent helps the preparation of homogeneous nano-particles. These results are in complete agreement with the structural analysis achieved by the XRD analysis.

The selected area electron diffraction (SAED) patterns of In_2O_3 nano-particles prepared by sol–gel and hydro-thermal methods have been shown in Fig. 6. The electron diffraction patterns of nano-particles represent a collection of halo-rings and discrete spots. Also, the SAED halo-ring patterns taken from nano-particles in both methods confirm that the product was well crystallized and the brightest ring corresponds to the (2 2 2) plane of In_2O_3. The comparison of the SAED patterns in Figs. 6(a) and (b) shows that in the sol–gel synthesis, the brightness of the rings and the order of spots are better than of the hydro-thermal method, which can be related to the utilization of the citric acid as complexing agent in sol–gel synthesis and hence production of the homogeneous In_2O_3 nano-particles.

The direct and indirect band gaps of the In_2O_3 nano-particles prepared by sol–gel and hydro-thermal methods have been presented in Figs. 7(a) and (b). The data for Fig. 7 have been obtained by optical absorption measurements and plotting $(\alpha h\nu)^2$

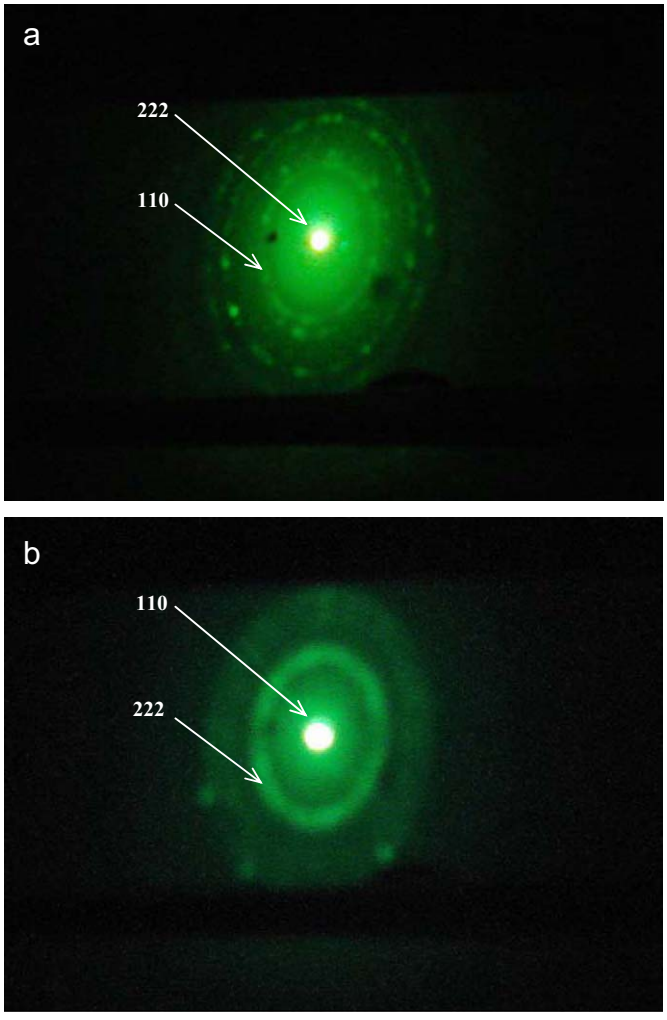

Fig. 6. The electron diffraction patterns of In_2O_3 nano-particles obtained by (a) sol–gel, and (b) hydro-thermal methods.

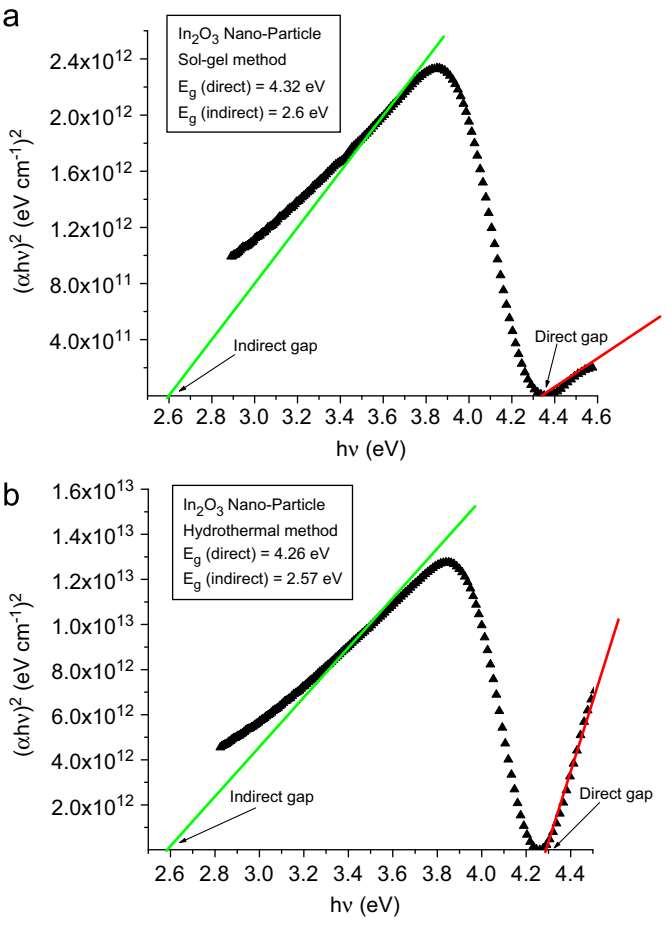

Fig. 7. The plot of $(\alpha h\nu)^2$ vs. hυ for In_2O_3 nano-particles: (a) sol–gel method and (b) hydro-thermal method, for determining the direct and indirect band gaps.

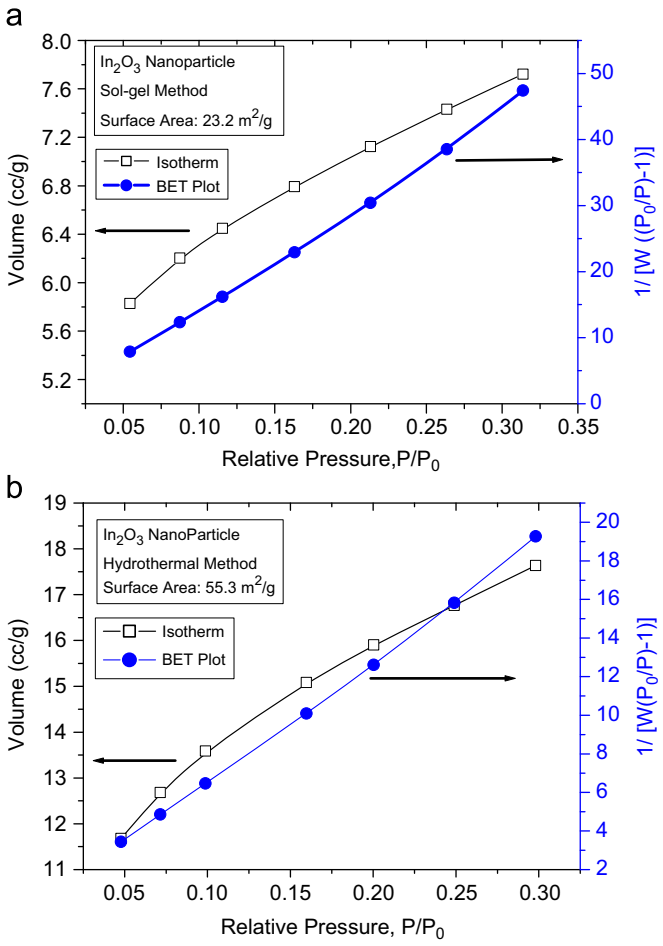

Fig. 8. Isotherm and BET plots vs. relative pressure for In_2O_3 nano-particles prepared by (a) sol–gel and (b) hydro-thermal methods.

vs. photon energy ($h\nu$); in which α, ν and h are the absorption coefficient, photon frequency, and the Planck's constant, respectively [21]. As shown in Fig. 7, the optical direct band gaps of nano-particles are 4.32 and 4.24 eV for sol–gel and hydro-thermal methods, respectively. These values exhibit about 0.5 eV blue shift from the bulk In_2O_3 (3.75 eV). Since the size of the particles is decreasing, and the atomic wave functions are overlapping more, we may attribute this to approaching to the quantum confinement limit of nano-particles. The quantum confinement effect is expected for the semiconducting nano-particles, and the absorption edge will be shifted to a shorter wavelength (higher energy) when the particle size decreases [18]. The indirect band gap value of In_2O_3 nano-particles is nearly 2.6 eV.

Figs. 8(a) and (b) show the isotherm and BET plots vs. relative pressure (P_0/P) for In_2O_3 nano-particles prepared by the sol–gel and hydro-thermal methods, respectively. As shown, both BET plots have linear behavior vs. relative pressure from 0.05 to 0.3. The values of the evaluated surface area of In_2O_3 nano-particles are 23.2 m^2/g for the sol–gel and 55.3 m^2/g for hydro-thermal method. The larger surface area obtained for the hydro-thermal method may be related to the presence of the In_2O_3 nano-particles with wire- or needle-like structures.

4. Conclusions

Indium oxide nano-particles have been successfully synthesized by two methods: sol–gel and hydro-thermal. The studies based on the XRD and TEM analyses show that in hydro-thermal method, the size range of the nano-crystallites (3–25 nm) is smaller than sol–gel method (10–45 nm). The XRD peaks of In_2O_3 nano-particles, prepared by the hydro-thermal method, are broader than ones obtained by the sol–gel method, because of the smaller size of the particles. The XRD results show that pure cubic phase in sol–gel synthesis and cubic-hexagonal mixed phase in hydro-thermal synthesis is obtained. The shape of nano-particles in sol–gel method is nearly spherical and in the hydro-thermal method we see neddle-like, wire-like grains with a homogeneous distribution of particles. The SEM images show that nano-particles prepared by both methods have grown as cluster or branch. Also, because of approaching the quantum confinement limit of the In_2O_3 nano-particles, a blue shift about 0.5 eV is observed in direct band gap of particles in comparison to bulk In_2O_3.

The results of surface area analysis of In_2O_3 nano-particles show that in the hydro-thermal method presence of particles with needle- and wire-like shapes may lead to larger surface area. Therefore, the hydro-thermal synthesis can be considered as a suitable synthesis route for sensing applications. Considering these results, we conclude that the type of synthesis route has an important role on the shape, morphology, and phase structure of In_2O_3 nano-particles. Therefore, by utilizing different synthesis methods, a variety of nano-particles with different structural properties can be obtained.

References

[1] A.L. Dawar, J.C. Joshi, J. Mater. Sci. 19 (1984) 1.
[2] H.L. Hartnagel, A.L. Dawar, A.K. Jain, C.J. Jagadish, Semi-conducting Transparent Thin Films, IOP, Bristol, 1995.
[3] B.G. Lewis, D.C. Paine, MRS Bull. 25 (8) (2000) 22.
[4] T.B. Elliott (Ed.), Trends in Semiconductor Research, Nova Science Publishers, New York, 2005.
[5] K.Y. Kim, S.B. Park, Mater. Chem. Phys. 86 (2006) 210.
[6] S.J. Limmer, K. Takahashi, G. Cao, Proc. SPIE 5224 (2003) 25.
[7] D. Yu, D. Wang, W. Yu, Y. Qian, Mater. Lett. 58 (2003) 84.
[8] H. Zhu, Y. Wang, N. Wang, Y. Li, J. Yang, Mater. Lett. 58 (2004) 2631.
[9] J.E. Song, Y.S. Kang, Proc. Mater. Res. Soc. Symp. 818 (2004) 1.
[10] S. Li, X. Qiao, J. Chen, H. Wang, F. Jia, X. Qiu, J. Cryst. Growth 289 (2006) 151.
[11] P.S. Devi, M. Chatterjee, D. Ganguli, Mater. Lett. 55 (2002) 205.
[12] Y. Li, G. Xu, Y.L. Zhu, X.L. Ma, H.M. Cheng, Solid State Commun. 142 (2007) 441.
[13] R. Garkova, G. Volksch, C. Russel, J. Non-Cryst. Solids 352 (2006) 5265.
[14] J.M. Kim, J.K. Park, K.N. Kim, C.H. Kim, H.G. Jang, Curr. Appl. Phys. 6S1 (2006) e198.
[15] A.M. Taurino, M. Epifani, T. Toccoli, S. Iannotta, P. Siciliano, Thin Solid Films 436 (2003) 52.
[16] M. Bhagwat, P. Shah, V. Ramaswamy, Mater. Lett. 57 (2003) 1604.
[17] S. Chaianansutcharit, O. Mekasuwandumrong, P. Prasertham, Ceram. Int. 33 (2007) 697.
[18] H. Zhu, D. Yang, G. Yu, H. Zhang, K. Yao, Nanotechnology 17 (2006) 2386.
[19] Z. Li, B. Hou, Y. Xu, D. Wu, Y. Sun, W. Hu, F. Deng, J. Solid State Chem. 178 (2005) 1395.
[20] X. Xiang, X. Zu, C.F. Zhang, S. Zhu, Q.M. Wei, K. Sun, L.M. Wang, Nanotechnology 17 (2006) 2636.
[21] E.A. Davis, N.F. Mott, Philos. Mag. 22 (1970) 903.